scientific reports

Check for updates

OPEN

Tailoring crosstalk between localized 1D spin-wave nanochannels using focused ion beams

Vadym Iurchuk[1]✉, Javier Pablo-Navarro[1], Tobias Hula[1], Ryszard Narkowicz[1], Gregor Hlawacek[1], Lukas Körber[1,2], Attila Kákay[1], Helmut Schultheiss[1], Jürgen Fassbender[1,3], Kilian Lenz[1] & Jürgen Lindner[1]

1D spin-wave conduits are envisioned as nanoscale components of magnonics-based logic and computing schemes for future generation electronics. *À-la-carte* methods of versatile control of the local magnetization dynamics in such nanochannels are highly desired for efficient steering of the spin waves in magnonic devices. Here, we present a study of localized dynamical modes in 1-μm-wide permalloy conduits probed by microresonator ferromagnetic resonance technique. We clearly observe the lowest-energy edge mode in the microstrip after its edges were finely trimmed by means of focused Ne^+ ion irradiation. Furthermore, after milling the microstrip along its long axis by focused ion beams, creating consecutively ∼50 and ∼100 nm gaps, additional resonances emerge and are attributed to modes localized at the inner edges of the separated strips. To visualize the mode distribution, spatially resolved Brillouin light scattering microscopy was used showing an excellent agreement with the ferromagnetic resonance data and confirming the mode localization at the outer/inner edges of the strips depending on the magnitude of the applied magnetic field. Micromagnetic simulations confirm that the lowest-energy modes are localized within ∼15-nm-wide regions at the edges of the strips and their frequencies can be tuned in a wide range (up to 5 GHz) by changing the magnetostatic coupling (i.e., spatial separation) between the microstrips.

Magnonic devices—often deemed the candidates for next generation electronics—take advantage of purely spin-based transport and processing of information encoded in the amplitude and/or the phase of spin waves, being the collective excitations of magnetization dynamics in thin films[1]. Increased endeavors have been taken to reduce the size and energy consumption of the magnonic blocks and enhance the control over the spin-wave propagation and their interaction with each other and with other components of the magnonic circuit[2]. Recent studies have successfully demonstrated possibilities to scale down magnonic waveguides to ∼50 nm in width by precise control of the nanofabrication conditions[3,4]. Another approach to reduce the lateral size of spin-wave conduits takes advantage of magnetic domain walls as propagation channels[5,6].

The tunable crosstalk between spin waves is a prerequisite of functional magnonic circuits like, e.g., nanoscale directional couplers and half adders[7], as well as periodic or quasi-periodic magnonic crystals[8]. In that respect, on-demand engineering of closely packed magnonic conduits is a key step towards controlling the magnetostatic interactions between spin waves[9–12]. One approach, allowing for such manipulation, lies in utilizing localized edge modes in patterned magnetic micro- and nanostructures[13–15]. A major weakness of this strategy is the fact that the experimental observation and manipulation of the edge-localized spin-wave modes is not straightforward due to excessive roughness of the edges of the structures fabricated by conventional methods. To overcome this drawback, material modification using focused ion beams (FIB)—in particular using Ne^+ ions from a Helium Ion Microscope (HIM)[16,17]—was recently employed for an on-demand precise manipulation of the magnetic nanostructure and shape to obtain high-quality edges[18,19]. On the other hand, conventional methods of magnetization dynamics detection are, in general, non-local, i.e., they are capable of probing the signal either from the whole structure (in case of conventional ferromagnetic resonance technique) or from a macroscopic region of

[1]Institute of Ion Beam Physics and Materials Research, Helmholtz-Zentrum Dresden-Rossendorf, 01328 Dresden, Germany. [2]Fakultät Physik, Technische Universität Dresden, 01062 Dresden, Germany. [3]Institute of Solid State and Materials Physics, Technische Universität Dresden, 01062 Dresden, Germany. ✉email: v.iurchuk@hzdr.de

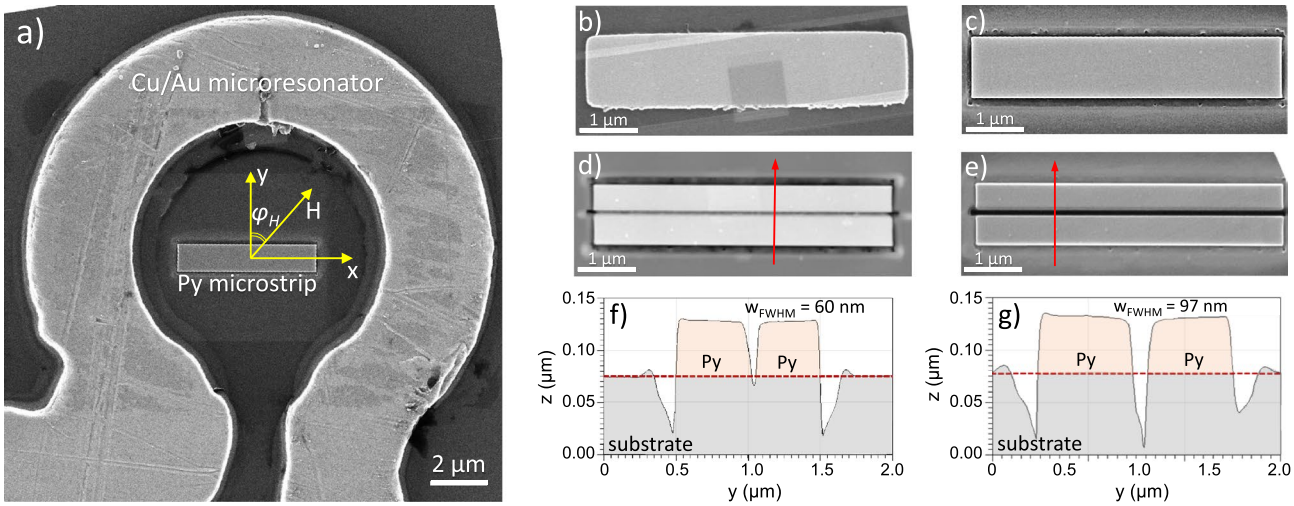

Figure 1. (**a**) Scanning electron microscopy (SEM) image of the Ω-shaped Cu/Au microresonator loop and the 5 µm × 1 µm × 50 nm Py strip sample positioned in the center. During the µFMR measurements, the static external magnetic field H is applied in-plane of the microstrip at angle ϕ_H with respect to the short axis of the strip. (**b**–**e**) SEM images of the (**b**) as-prepared Py microstrip, (**c**) edge-trimmed using Ne-FIB, (**d**) cut along by Ne-FIB leaving a nominal gap of 50 nm and (**e**) 100 nm. (**f**, **g**) Atomic force microscopy (AFM) profiles of the cut strips measured along the red arrows shown in (**d**) and (**e**), respectively. Dashed lines indicates the substrate level.

the sample (in case of conventional Brillouin light scattering technique). When applied to the arrays of closely spaced magnetic objects, these methods detect an averaged dynamical signal and, therefore, meet difficulties in resolving the magnetization dynamics of an individual structure.

Here, we present a compound study of the magnetization dynamics in a single confined micron-sized permalloy (Py) strip as a function of its shape, modified on-demand by means of focused Ne^+ ion beam milling. More specifically, we use planar microresonator ferromagnetic resonance (µFMR) spectroscopy complemented by Brillouin light scattering (BLS) microscopy and micromagnetic simulations to investigate the dynamics of a single 5 µm × 1 µm × 50 nm strip. The study has been performed for the strip in an as-prepared state as well as cut along its length using Ne-FIB, creating consecutively two 5-µm-long strips separated by 50 and 100-nm-wide gaps, respectively. We show that HIM-based modification of the Py microstrip geometry directly impacts the dynamical spectra, i.e., it leads to the appearance of additional resonances in the corresponding spectra. Using micromagnetic modelling, we have attributed these resonances to the dynamical modes localized at the narrow regions of the inner edges of the cut strips. We demonstrate that the resonance fields of these modes can be effectively tuned by changing the distance between the two strips. We further confirm the localization of the emerged modes by BLS microscopy showing good agreement with the µFMR measurements. Our analysis shows that Ne-FIB-assisted modification of confined magnetic microstructures constitutes a powerful tool for the on-demand control of the magnetization dynamics in closely packed magnonic conduits.

Results and discussion

Sample fabrication and Ne-FIB milling procedure. Figure 1a shows a scanning electron microscopy (SEM) image of the fabricated device comprising a 50-nm-thick Py microstrip with 5 µm × 1 µm nominal planar dimensions, centered inside the Ω-shaped loop of the microresonator (see section "Methods" for the fabrication details). Figure 1b shows an SEM image of the as-prepared Py microstrip with clearly visible imperfections on the edges formed naturally during standard wet lithography processing. We use focused ion beam-assisted milling by means of a Neon gas field ion source (GFIS) of a Zeiss Orion NanoFab[17] to obtain a precise modification of the microstrip shape (see section "Methods"). Figure 1c shows an SEM image of the Py microstrip after its edges were trimmed by Ne-FIB in order to obtain smooth sidewalls with minimum irregularities. Thereafter, the central region along the strip was milled in order to obtain two strips separated by a gap of nominal 50 nm width [see Fig. 1d]. Finally, the milled gap was widened to nominal 100 nm width [see Fig. 1e]. To confirm the quality of the Ne-FIB-based milling and to visualize the cross-section of the cut strips, we performed atomic force microscopy (AFM) linescans across the Py microstrips [red arrows in Fig. 1d,e indicate the scan directions].

The AFM measurements on the strips with nominal 50 nm and 100 nm gaps [see Fig. 1f,g, respectively] confirm the high quality of the Ne-FIB milling procedure allowing for the smooth shaping of both inner and outer edges of the strips. However, due to inevitable straggling of the Ne ions and AFM-tip artifacts in the narrow trench, the inner edges are not straight and appear to have a rather quasi-Gaussian cross-section profile at the bottom. Nonetheless, the measured full-width-half-maximum of the fabricated gaps is 60 nm and 97 nm for the nominal gap width of 50 nm and 100 nm, respectively [see Fig. 1f,g].

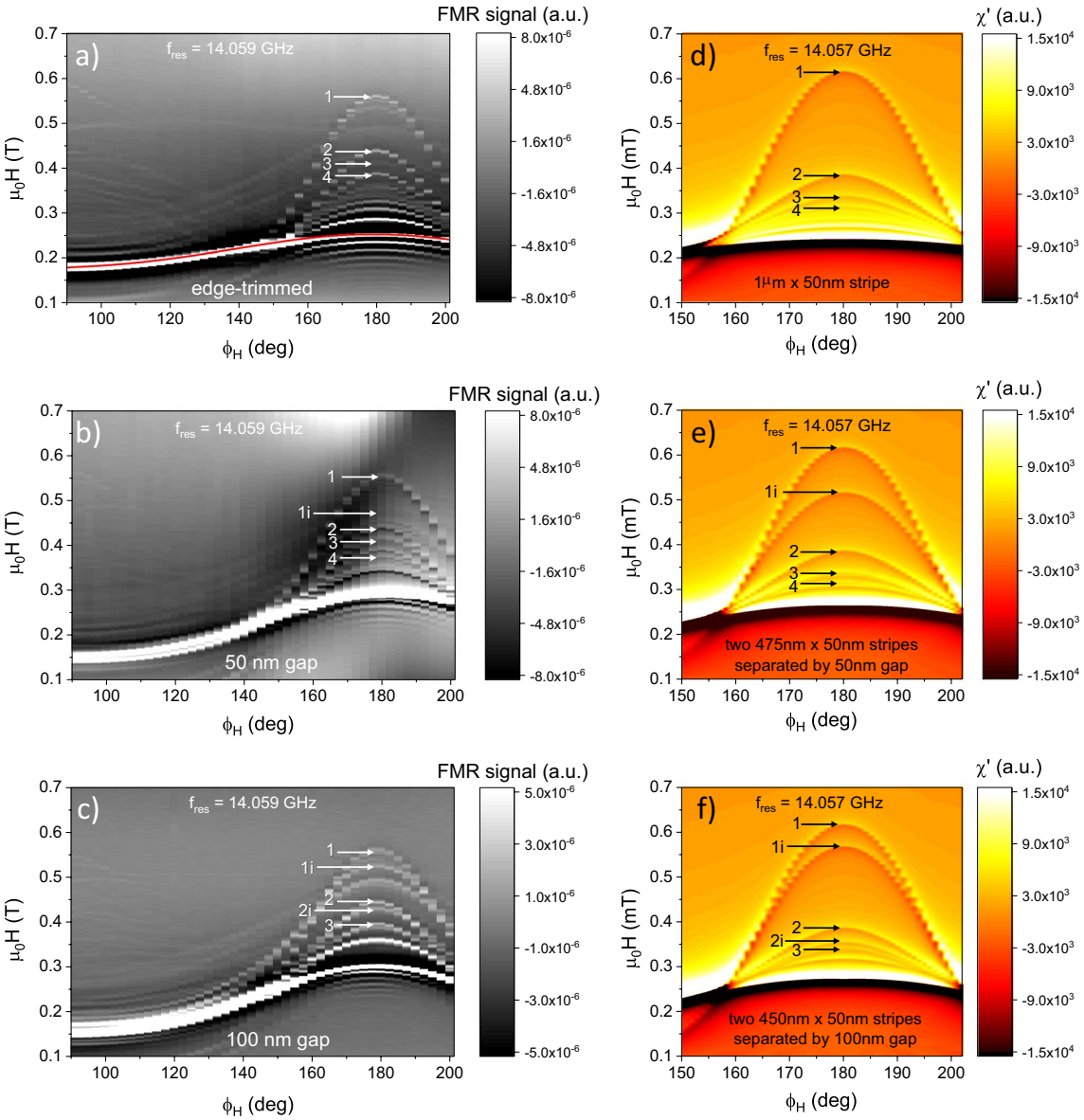

Figure 2. (**a**–**c**) In-plane angular dependences of the field-swept µFMR signal measured at 14.059 GHz for (**a**) the edge-trimmed microstrip, (**b**) cut along in half using the Ne-FIB with a nominal gap of 50 nm, and (**c**) 100 nm. The red line in (**a**) shows the analytical fit to the measured data using the Kittel relation. The edge modes are numbered in the order of their appearance starting from the high field values (see text for details). (**d**–**f**) Corresponding µFMR spectra of an infinitely long strip simulated for the excitation frequency of 14.057 GHz. (**d**) Infinitely long 1-µm-wide and 50-nm-thick strip, (**e**) two 475-nm-wide infinitely long strips separated by 50 nm, and (**f**) two 450-nm-wide strips separated by a 100-nm-wide gap.

µFMR measurements. After each FIB modification, µFMR measurements were performed to probe the dynamical modes associated to the corresponding shape of the sample [as-prepared (not shown), edge-trimmed, with a 50-nm-wide gap and a 100-nm-wide gap]. The lowest-energy localized edge mode can hardly be detected in the as-prepared microstrip. Indeed, as shown by McMichael et al.[20], the edge-mode resonance field is extremely sensitive to the quality of the strip sidewalls. Excessive roughness, oblique sidewalls and local deviations of the saturation magnetization at the edges of the as-prepared strip lead to considerable decrease of the edge-mode resonance field. Additionally, due to its localized nature, the lowest-energy edge mode has lower amplitude as compared to the other resonances in a magnetic strip. Moreover, considerable edge roughness of the as-prepared strip leads to slight deviations of the resonance field and, therefore, to the broadening of the edge mode resonance due to local variations of the effective magnetic field associated with the edge shape inhomogeneities. However, similar to the work presented by Lenz et al.[18], this mode is clearly observed when the edges of the microstrip are finely trimmed by focused Ne ion beams. Figure 2a shows the µFMR signal for an in-plane field sweep measured on the edge-trimmed Py microstrip [see Fig. 1c] at f_{res} = 14.059 GHz for different angles of the in-plane bias field ϕ_H ranging from 90° to 202°. When the bias field is parallel to the strip, i.e., ϕ_H = 90°, the µFMR signal exhibits a strong peak around 180 mT corresponding to the main dynamical mode

excited in the center of the strip. As the applied magnetic field is rotated towards the direction perpendicular to the strip ($\phi_H = 180°$), a rich field-dependent mode structure emerges. At $\phi_H = 180°$, the mode 1 with the highest resonance field (here $\mu_0 H_{res} = 557$ mT) corresponds to the *true edge* mode localized at the very edge of the long side of the strip[18]. Subsequent modes appearing at $\mu_0 H_{res} = 437$ mT, 408 mT and 385 mT are attributed to the mode 2, mode 3 and mode 4 localized in the vicinity of the strip edge, respectively. One should not confuse these resonances with the higher-order modes of the true edge mode. These localized modes are essentially confined standing spin waves. A rigorous theoretical description of the spin-wave resonances in confined Py microelements is given by Bayer et al. in Ref. [21], where a detailed classification of the exchange-dominated edge modes and dipolarly-dominated center modes is presented and their frequency-field characteristics are derived. The detailed quantification of the mode character will be discussed further in section Dynamical modes definition.

When the field orientation is deviating from the $\phi_H = 180°$ direction (across the strip), the effective magnetic field increases due to the dipole-dipolar energy contribution. Therefore, at a given frequency, the resonance fields of the corresponding modes downshift towards lower values. At $\phi_H \sim 150°$, the effective external field in the direction perpendicular to the strip becomes lower than the energy threshold required for the edge mode's stability, and the edge modes vanish.

Figure 2b,c show the μFMR signal measured on the Py microstrip cut in the middle by Ne-FIB to obtain two 5 μm long strips separated by a nominal 50 nm and 100 nm gap, respectively. A qualitative comparison of the angle-dependent μFMR spectral maps of the strips reveals additional modes appearing in the region of the spectral band corresponding to the large ϕ_H angles as compared to the edge-trimmed strip. However, we observe not only the overall shift of the resonance fields of the dynamical modes due to the modified magnetostatic energy of the system, but also a pronounced splitting of the edge-mode resonances. To identify the origin of the measured modes in detail, we use micromagnetic simulations as well as BLS microscopy. As explained further in section Dynamical modes definition, the emerged additional modes shown in Fig. 2b,c can be attributed to the ones localized at the *inner edges* of the fabricated strip pairs (marked with 'i') as opposed to the ones localized at the *outer edges* (marked with numbers only), which are already visible in the edge-trimmed strip as well. The complementary BLS measurements allow for a visualization of the localization of the modes that can directly be compared with the simulated mode profiles.

Micromagnetic simulations. To reveal the dynamical mode profiles and to define the exact localization of the modes within the strips, we have performed micromagnetic simulations of the magnetization dynamics in confined Py microstrips using the two-dimensional propagating-wave eigensolver of the open source finite-element micromagnetic package TetraX[22,23]. First, we simulated the absorption spectra[24,25] of the infinitely long Py strip with a 1 μm × 50 nm cross section. To mimic the μFMR measurements on the Ne-FIB-cut strips, we performed similar simulations of the pairs of infinitely long strips with 475×50 nm^2 and 450×50 nm^2 cross sections spaced laterally by 50 nm and 100 nm, respectively. For all simulations, the static magnetic field was applied in the sample plane, and the absorption was computed assuming a homogeneous out-of-plane rf field profile.

Figure 2d–f show the μFMR absorption spectra for an excitation frequency of $f = 14.057$ GHz and for different azimuthal angles ϕ_H of the in-plane field. Here, we have simulated the magnetization dynamics in three different strip geometries: Fig. 2d shows the result of an infinitely long, 1 μm wide and 50 nm thick strip, Fig. 2e shows two 475-nm-wide infinitely long strips separated by a 50-nm-wide gap and Fig. 2f two 450-nm-wide strips separated by a 100 nm gap, respectively. These data are in good agreement with the experimentally measured μFMR spectra of Fig. 2a–c. More specifically, the simulated ϕ_H angular dependence of the FMR signal of the edge-trimmed strip reveals a band of excited dynamical modes whose resonance fields $\mu_0 H_{res}$ decrease with increasing mode number [see Fig. 2d]. The first four resonances are observed at $\mu_0 H_{res} = 614$ mT, 383 mT, 335 mT and 231 mT, respectively. The angular dependence directly correlates with the experimental data, exhibiting a resonance field downshift with increased deviation from the $\phi_H = 180°$ azimuthal direction of the bias field.

A similar distribution of the modes is observed in the simulated FMR spectra of the cut strips, i.e., the appearance of the additional modes at bias fields, which do not match the resonances of the main mode numbers. The origin of these modes is attributed to the magnetostatic coupling between the closely spaced strips. For example, for a 50 nm gap, the first additional mode (labeled as mode 1i) appears at $\mu_0 H_{res} = 515$ mT, i.e., between the resonance fields of the mode 1 and the mode 2, and separated by 100 mT from the mode 1 resonance. Similarly, for the 100-nm-wide gap, the mode 1i is observed at $\mu_0 H_{res} = 567$ mT, being separated by 50 mT from the corresponding resonance field of the true edge mode. This frequency separation between the first two resonances observed in the cut strips decreases with increasing gap-width due to a decreasing magnetostatic coupling between the strips, and eventually vanishes for gaps wider than ~500 nm (not shown here). For such large spacing, the magnetization dynamics in both strips were found to be essentially independent, as the strips become magnetically isolated due to the negligible magnetostatic coupling between them. For the lower magnetic field values, a distinct splitting of the dynamical modes is observed too, whose classification is presented in the next section.

Dynamical modes definition. To classify the observed modes and define the distribution of the dynamic magnetization profile within the cut strips, we examined the μFMR spectra for the fixed azimuthal angle of $\phi_H = 180°$ [Fig. 3a] and compared them to the corresponding simulated spectra [Fig. 3b] and extracted mode profiles [Fig. 3c–e].

The experimental μFMR spectrum of the edge-trimmed strip (top green curve) in Fig. 3a shows multiple resonances, and the corresponding simulated spectrum in Fig. 3b allows for attributing the observed resonances to well-defined mode profiles as depicted in Fig. 3c. Note that we plot the field-derivative of the FMR dispersion signal ($d\chi'/dH$) giving a symmetric peak to make the peaks easily identifiable by their local maximum. While decreasing the field from saturation, we observe the first distinct μFMR peak at $\mu_0 H_{res} = 557$ mT. Comparing

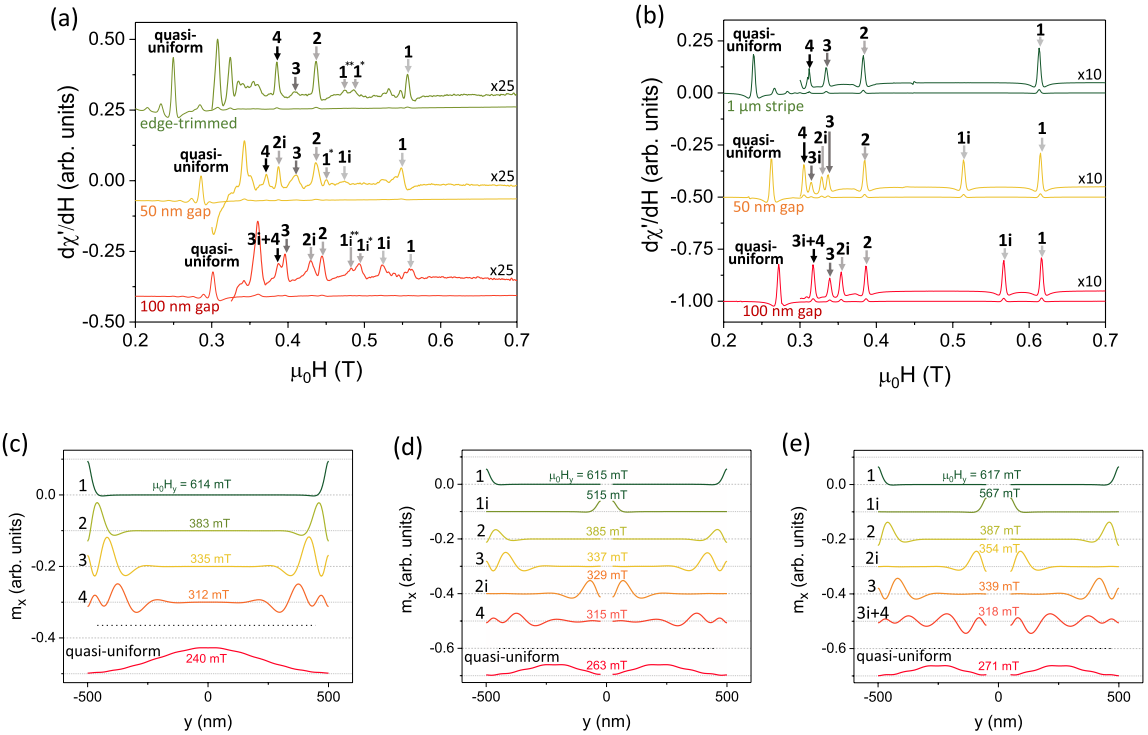

Figure 3. (**a**) Field-swept μFMR spectra measured for $\phi_H = 180^\circ$ on the edge-trimmed strip (top green curve), and cut with 50 nm (middle yellow curve) and 100 nm gaps (bottom red curve), respectively. (**b**) Corresponding simulated FMR spectra of an infinitely long strip with 1 μm × 50 nm cross section, two strips with 475 nm × 50 nm cross section separated by 50 nm, and two strips with 450 nm × 50 nm cross section separated by 100 nm gap, respectively. The spectra in (**a**) and (**b**) show the field-derivative of the dispersion signal $d\chi'/dH$ and are vertically offset for visual clarity. Numbers in (**a**) and (**b**) denote the mode order (see text). (**c**–**e**) x-components of the mode profiles of the single strip (**c**) and HIM-cut strips (**d**, **e**) for the bias field values corresponding to the resonances observed in **b**). The linescans are vertically offset for better visualization.

the position of this peak with the simulations, and visualizing the mode profile of the corresponding mode, we attribute this resonance to the mode 1, i.e., the true edge mode localized at the long edges of the strip. Detection of this mode by conventional inductive FMR measurements is often elusive due to its reduced active mode volume in confined geometries and very sensitive dependence of the signal on the quality of the sample edges. Nevertheless, our μFMR technique with optimized filling factor of the microresonator allows for the detection of such low energy modes[18]. Notably, the dynamical magnetization profile of this mode is extremely localized in the narrow edge region of the strip within a width of ~15 nm.

By further decreasing the bias field, we observe additional localized resonances, which appear consecutively at $\mu_0 H_{\text{res}} = 437$ mT, 408 mT and 385 mT. These resonances are also present in the simulated data, allowing for a classification of the observed modes by examining their dynamical profiles. One can see in Fig. 3c that the mode 2 profile is no longer perfectly localized at the edges of the strip, but moves towards the center of the strip. The consecutive modes also exhibit periodic magnetization pattern with the tendency of shifting their maximum precession amplitude towards the center of the strip. Upon lowering the field, the amplitudes of the observed peaks increases, and the spreading and hybridization of the dynamical nodes within the strip do not allow for exact classification of the measured mode. These modes, contrary to the Kittel-like true edge mode, correspond to standing spin-wave resonances, confined in specific regions of the strip. Indeed, as shown by Pile et al.[26], with decreasing field, these regions of the mode localization shift from the edges towards the center of the strip, where two counter-propagating spin waves form quantized nodes.

Eventually, when reaching the value of the main FMR resonance, we observe a large-amplitude signal at $\mu_0 H_{\text{res}} = 249$ mT, attributed to the quasi-uniform resonance mode after visualizing its simulated mode profile [see Fig. 3c]. We note that the low amplitude resonances observed for the edge-trimmed strip between ~450 and ~500 mT, and labeled as modes 1* and 1**, were not reproduced in the micromagnetic simulations [see top green curve in Fig. 3b]. Possible sources of these peaks may be attributed to the non-uniform thickness of the edge-trimmed strip, asymmetry of the opposite edge shapes, and/or edge inhomogeneities due to the ion-induced modification of the Py microstructure or due to the material redepositions during the milling.

A more complex set of dynamical modes is observed in the cut strips, where the additional peaks emerge in both experimental and simulated μFMR spectra. More specifically, for a 50 nm gap between the strips, a pronounced peak appears at $\mu_0 H_{\text{res}} = 474$ mT [see middle yellow curve in Fig. 3a]. A similar peak is also observed in the simulated spectra at $\mu_0 H_{\text{res}} = 515$ mT [see middle yellow curve in Fig. 3b]. When visualizing the mode profile of this resonance [see Fig. 3d], we can clearly attribute it to the so-called mode 1i, i.e., the first edge mode

localized at the *inner* edges of the two strips after the milling. Upon further decrease of the bias field, we observe the peak at $\mu_0 H_{res}$ = 436 mT attributed to the mode 2, which is localized at the *outer* edges of the cut strip, as confirmed by the micromagnetic modelling of the corresponding mode profiles. Further reducing of the bias field reveals a resonance at $\mu_0 H_{res}$ = 410 mT, which was expected to be associated with the mode 2i. Surprisingly, the micromagnetic analysis shows that for the pairs of 475-nm-wide strips separated by a 50 nm gap, this mode has a lower resonance field, therefore, higher frequency as compared to mode 3. Detailed examination of the mode profile of this particular resonance confirms that the resonant response is localized in the vicinity of the outer edges, and the alternation of the precession maxima and minima allows for an unambiguous classification of the observed mode as mode 3. The resonance mode 2i for this particular geometry appears between the resonant fields of the modes 3 and 4 [see the resonances of the yellow curve in Fig. 3a,b and the corresponding mode profiles in Fig. 3d]. The origin of this behavior is attributed to the reduced outer edges saturation field due to the increased magnetostatic coupling between the strips. The quasi-uniform mode is detected via μFMR at $\mu_0 H_{res}$ = 286 mT, following the global shift of the resonance fields due to the modified shape anisotropy as compared to the uncut strip. The corresponding difference in the anisotropy fields, extracted from the micromagnetic simulations, is ~25 mT, which is in good agreement with the experimentally observed values.

When the gap between the two strips increases to 100 nm [see bottom red curve in Fig. 3a], the resonances of the corresponding inner edge modes are shifted towards the outer edge mode resonances due to the decreased magnetostatic coupling in the system of two strips. More specifically, the resonance 1i is now detected at $\mu_0 H_{res}$ = 523 mT, i.e., closer to the mode 1 resonance as compared to the 50 nm gap. Upon decreasing bias field, we observe resonance mode 2 at $\mu_0 H_{res}$ = 444 mT followed by mode 2i at $\mu_0 H_{res}$ = 429 mT. The same is true for mode 3i, which now is located straight below mode 3. Notably, at first glance, we were unable to resolve a distinct peak of mode 4 in our μFMR measurements. However, an analysis of the simulated mode profiles reveals a superposition of the modes 3i and 4 [see Fig. 3e], i.e., the resonant response of both modes occurs at the same field value, $\mu_0 H_{res}$ = 387 mT. The corresponding mode profile shows the features of the mode 3i localized closer to the inner edges of the strips, and the mode 4, which is located closer to the outer edges of the strips. This superposition is the consequence of the reduced width of the strips, where the spatially distributed dynamical magnetization of the two different but closely spaced eigenresonances can be excited at the single resonance frequency in the confined geometry at the given magnetic field. In general, fine adjustment of the strip geometry and separation enables a simultaneous excitation of the modes with different mode numbers, localized at inner and/or outer edges of the cut strips at given frequency, if their resonance fields match.

One has to comment on the two additional modes present in the experimental μFMR spectrum of the strips with 100 nm gap at $\mu_0 H$ = ~490 mT denoted as 1i* and 1i** in the bottom curve of Fig. 3a. Although these resonances were not observed in the simulations, the spatially resolved BLS microscopy measurements presented in the next section show that these modes are also localized at the inner edges of the cut strips.

One can see that the difference between the experimental and the simulated values can reach tens of mT. Here, we comment on the possible origins of these discrepancies. First, the TetraX simulation framework allows working with exclusively 2D geometries, which automatically sets one of the demagnetizing factors (here, N_x) to zero, thus lowering the in-plane shape anisotropy, which leads to increased $\mu_0 H_{res}$ values when the transverse bias field is applied to the strip. Second, as can be seen from the topography of the cut strips [see AFM scans in Fig. 1f,g], the profile of the outer and, especially, inner edges is not straight, but significantly deviates from the vertical. This results in a non-uniform separation between the strips across the thickness. For example, for the 100-nm-nominal-gap width, the separation between the strips is ~60 nm at the substrate level and ~130 nm at the top surface of the Py strip. The oblique shape of the edges leads to a considerable redistribution of the edge mode's localization within the inner edge of the cut strips and, therefore, to the shift in the corresponding resonant magnetic fields. Third, the position of the edge mode resonances is extremely sensitive to the asymmetries in the system introduced by the FIB milling. The asymmetric profiles of the gap sides together with the difference in the widths of the cut strips may contribute to the resonance field shift due to the relocalization of the modes within the strips. The described inhomogeneities can also be considered as the origin of the appearance of modes 1i* and 1i**.

Brillouin light scattering microscopy. To further elucidate the mode localization within the strips experimentally, we measured the spin-wave spectra on the strip with the 100-nm-wide gap by means of Brillouin light scattering (BLS) microscopy[27]. The BLS was performed on the same sample as the μFMR using an excitation frequency of f_{res} = 14.059 GHz.

Figure 4a shows the spatially resolved BLS intensity map as a function of the laser spot position for different bias magnetic fields applied perpendicular to the strip's long axis ($\phi_H = 180^\circ$). Depending on the magnetic field magnitude and the position of the beam, one can clearly distinguish the different resonances, which directly correspond to the modes defined in the previous section for the strips with a 100 nm gap. More specifically, the large amplitude resonance around $\mu_0 H$ = 300 mT is attributed to the quasi-uniform (center) mode. The BLS intensity vs. beam position across the strip as plotted in Fig. 4b confirms that this mode is essentially spread over the whole strip width with the maximum amplitude in the center of the individual strips. The spatial distribution of the dynamical response is in agreement with the simulated mode profile of the quasi-uniform FMR mode shown in the bottom-most image of Fig. 3e.

With increasing magnetic field, we can clearly identify the other modes present in the system. By examining their BLS intensity distributions across the strip width and comparing the resonance fields with the ones measured by μFMR, we can attribute the detected resonances to the corresponding edge modes of the strips. For example, Fig. 4c shows the measured BLS intensity across the structure for $\mu_0 H$ = 551 mT (black circles) and $\mu_0 H$ = 508 mT (red squares). The distribution of the BLS intensity across the strip width confirms that the detected

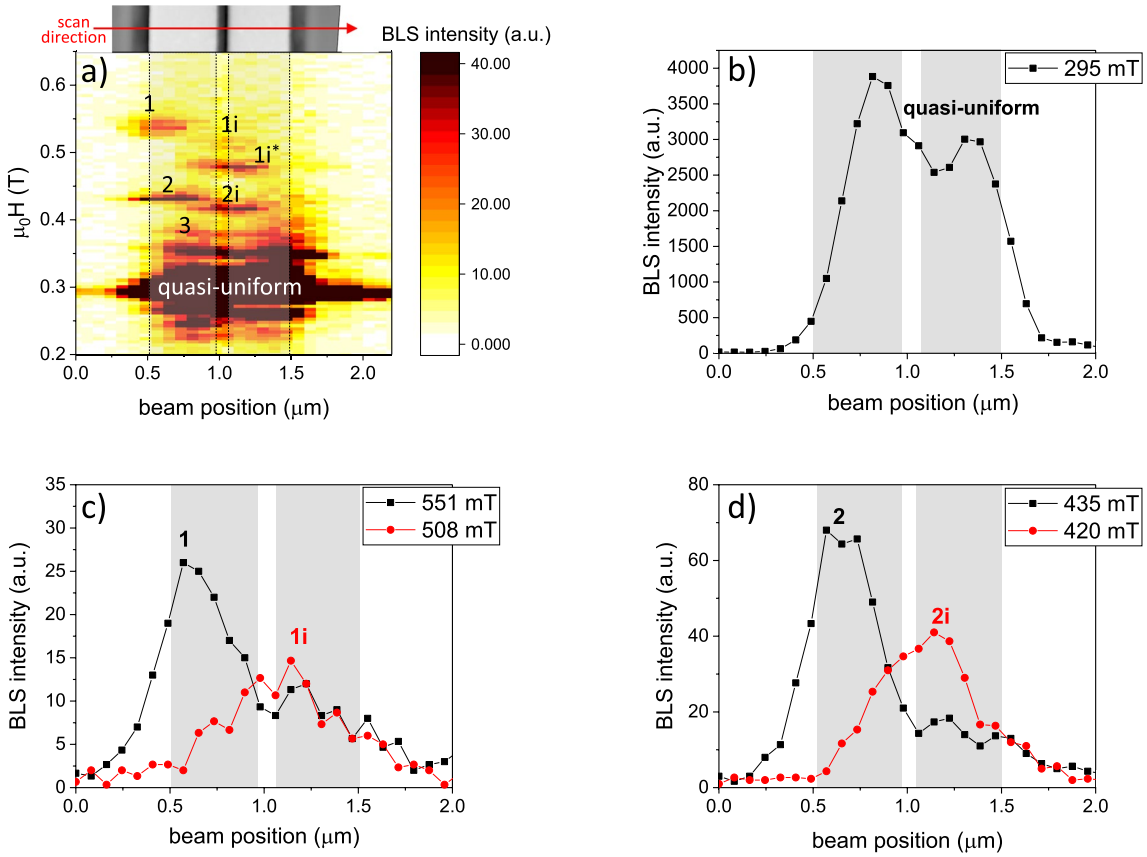

Figure 4. (**a**) BLS intensity map measured on the HIM-cut strip with 100 nm gap as a function of the in-plane bias field applied perpendicular to the strip's long axis and for different laser beam positions across the sample (denoted by the red arrow in the top inset). The measurements were performed at an excitation frequency of 14.059 GHz. Rectangles on the map are guides to the eye to indicate the strip edges. (**b**) BLS intensity as a function of the beam position measured for $\mu_0 H$ = 295 mT, corresponding to the quasi-uniform μFMR mode. (**c**, **d**) BLS intensity vs. beam position measured for the fields corresponding to (**c**) the modes 1 and 1i and (**d**) the modes 2 and 2i localized at the outer (black circles) and the inner (red squares) edges of the cut strips, respectively. The shaded rectangles in (**b**–**d**) denote the positions of the strip cross sections with respect to the scanned range.

modes correspond to the mode 1, localized at the outer edge of the strip, and mode 1i, localized at the inner edges of the strips. The same analysis allows for classifying the modes at $\mu_0 H$ = 435 mT and $\mu_0 H$ = 420 mT as modes 2 and 2i, respectively [see Fig. 4d]. In addition, one can clearly note the gradual shift of the BLS intensity of the localized modes towards the central region of the strip, in accordance with the simulated mode profiles of Fig. 3e. Despite limited spatial resolution of the BLS microscopy [taking into account the positioning stage step of ~80 nm (for this particular experiment) and the laser beam spot size of ~350 nm (see section "Methods"], a comparison of μFMR and BLS with the corresponding simulated mode profiles allows for an unambiguous classification of the visualized resonances.

Notably, the modes 1i* and 1i**, present in the μFMR spectra, are also detected by the BLS microscopy [see Fig. 4a]. The spatial distribution of their BLS intensity signal indicates that these modes are localized at the inner edges of the strips. Therefore, the appearance of these modes is attributed to the inner edges asymmetry of the cut strips (including a non-uniform separation over the thickness and side wall slope), as explained above in section Dynamical modes definition.

Interestingly, the modes localized at the outer edges are detected only at one side of the strip. This asymmetry might be explained by a non-homogeneous rf field distribution across the strips due to the slight off-center position of the strips in the microresonator. Therefore, opposite strip edges are exited with different rf-field amplitudes leading to the spatial asymmetry of the BLS intensity map. Additionally, the Ω-shaped antenna has a ~2 μm opening to allow for the rf current flowing through the resonator [see Fig. 1a]. Hence, the strip edge closer to this opening is excited with different amplitude as compared to the opposite edge, and the corresponding dynamical signal falls below the detection threshold.

One has to note that the slight discrepancies between the resonance fields detected by μFMR and BLS measurements can be attributed to different scales of the experiments. Whereas in the inductive μFMR measurements a volume-averaged magnetic signal is detected, the BLS microscopy is a purely local technique probing the dynamics in the small area illuminated by the laser spot. In that respect, laser-induced heating of the sample may also contribute to the observed resonance fields shift due to locally modified magnetic parameters. In addition,

the BLS signal acquires the whole band of the excited resonances at different k vectors for a given excitation frequency, whereas the μFMR is sensitive to uniform magnetization dynamics. Nevertheless, a good qualitative agreement between both experiments allows one to associate the observed resonances to the corresponding localized modes measured in the pair of Py strips.

Conclusions

This work takes advantage of different techniques, i.e., micro-cavity FMR spectroscopy, BLS microscopy, and micromagnetic modelling, to study the magnetization dynamics in confined magnetic microstructures modified by Ne^+ GFIS-based FIB(HIM). We have demonstrated that ion-induced modification of the magnetic microstructure geometry directly alters the ferromagnetic resonance band structure. When the 5 μm × 1 μm × 50 nm Py microstrip is cut into two strips along its length, additional resonances emerge in the corresponding μFMR spectra, attributed to the dynamical modes localized in the narrow (∼15 nm) regions of the inner edges of the cut strips. Local probing by means of BLS microscopy shows a good agreement with the μFMR data and confirms the modes localization at the inner/outer edges of the cut strips. Micromagnetic modelling using the 2D eigensolver of the TetraX package helps to identify the observed modes. Moreover, preliminary micromagnetic studies show that the inner edge-mode resonance fields can be tuned in a wide range by controlling the spatial separation between the strips. For example, resonance mode 1i shifts up by 173 mT (at 14.059 GHz) when going from a 20-nm to a 200-nm-gap between the strips, which corresponds to a ∼5.5 GHz shift in the frequency domain at fixed bias field.

In conclusion, Ne-FIB-assisted modification of the magnetic micro- and nanostructures is a powerful method of tailoring the nanoscale spin-wave channels with tunable coupling and dynamical properties. Such combined experimental approach allows for a complex characterization of the magnetization dynamics in the closely packed confined magnetic structures fabricated on-demand using focused ion beams.

Methods

Sample fabrication. The Ω-shaped microresonator was fabricated on highly resistive Si(001) substrate by means of conventional UV lithography followed by a deposition of Cr(5 nm)/Cu(600 nm)/Au(100 nm) by e-beam evaporation and lift-off. The back side of the substrate was metallized with Cr(5 nm)/Cu(300 nm)/Au(100 nm) to create a ground plane for the microresonator. The detailed description of the microresonator design and fabrication process can be found elsewhere[28,29]. As a next step, the Py microstrip was prepared using e-beam lithography, thermal evaporation and lift-off.

Helium ion microscopy based milling. A Ne gas field ion source (GFIS) based FIB (Helium Ion Microscope[16] Zeiss Orion NanoFab) was used for the modification of the Py microstrip. For the milling, we used Ne^+ ions with a kinetic energy of 25 keV, a 10 μm aperture and a spot control of 5. This resulted in an ion beam current of 1.3 pA. A fluence of 5000 ions/nm^2 has been applied for milling the structures.

μFMR measurements. The FMR was measured using a home-built FMR spectrometer. The field-sweept μFMR measurements were performed for different angles ϕ_H of the bias magnetic field H applied in the plane of the Py microstrip [see Fig. 1a]. The out-of-plane rf magnetic field is generated by injecting rf currents into the Ω-shaped antenna. The geometry of the rf circuit was designed to yield an out-of-plane microwave excitation field with the resonant frequency of 14.059 GHz and a maximum rf amplitude of $\mu_0 h_{rf}$ = 0.65 mT at 85 μW of injected rf power. More details on the μFMR technique can be found in Refs.[28,30,31].

Micromagnetic simulations. We calculate the eigenvalues and the corresponding eigenstates of the Py strips for different orientations and magnitudes of the bias magnetic field using the open source finite element method package TetraX[22,23]. By fitting the angle-dependent μFMR of the edge-trimmed Py using the Kittel relation [marked by the red curve in Fig. 2a], the following magnetic parameters of the Py strip were extracted: saturation magnetization M_s = 760 kA/m and the g-factor g = 2.11 corresponding to the reduced gyromagnetic ratio $\gamma/2\pi$ = 29.547 GHz/T. We also used the exchange stiffness A_{ex} = 13 pJ/m and the damping constant α = 0.008 for the simulations. For each geometry, a triangular mesh with cell size of 5 nm was used. To visualize the angular dependence of the FMR resonance field $\mu_0 H_{res}$, we first calculate the frequency-swept absorption spectra as a function of the magnitude and the direction of the bias magnetic field. Then, we extract the field-swept absorption spectra and compute their derivatives for different azimuthal angles ϕ_H at f_{res} = 14.057 GHz corresponding to the experimental resonance frequency of the μFMR microcavity circuit.

BLS microscopy. For the μ-BLS measurements, a 532 nm continuous-wave laser was focused to a spot size of approximately 350 nm and scanned across the strips using a high precision positioning system with a spatial precision of ∼10 nm. The laser power on the sample surface was about 1 mW. The magnetization dynamics was excited by passing an rf current with 12 dBm power through the Ω-shaped antenna. We have performed a line scan in the central region of the strips as shown in the top inset of Fig. 4a, where the red arrow denotes the scanning direction. The frequency and the intensity of the inelastically scattered light were analyzed using a high contrast Tandem-Fabry-Pérot interferometer. See Ref.[27] for more details on BLS microscopy.

Data availability

The datasets used and/or analysed during the current study are openly available in RODARE[32].

Received: 6 October 2022; Accepted: 28 December 2022
Published online: 14 January 2023

References

1. Barman, A. The. *et al.* Magnonics roadmap. *J. Phys. Condensed Matter* **33**, 413001. https://doi.org/10.1088/1361-648X/abec1a (2021) (**Publisher: IOP Publishing**).
2. Chumak, A. V. *et al.* Advances in magnetics roadmap on spin-wave computing. *IEEE Trans. Magnet.* **58**, 1–72. https://doi.org/10.1109/TMAG.2022.3149664 (2022) (**Conference Name: IEEE Transactions on Magnetics.**).
3. Wang, Q. *et al.* Spin pinning and spin-wave dispersion in nanoscopic ferromagnetic waveguides. *Phys. Rev. Lett.* **122**, 247202. https://doi.org/10.1103/PhysRevLett.122.247202 (2019) (**Publisher: American Physical Society.**).
4. Heinz, B. *et al.* Propagation of spin-wave packets in individual nanosized yttrium iron garnet magnonic conduits. *Nano Lett.* **20**, 4220–4227. https://doi.org/10.1021/acs.nanolett.0c00657 (2020) (**Publisher: American Chemical Society**).
5. Garcia-Sanchez, F. *et al.* Narrow magnonic waveguides based on domain walls. *Phys. Rev. Lett.* **114**, 247206. https://doi.org/10.1103/PhysRevLett.114.247206 (2015) (**Publisher: American Physical Society**).
6. Wagner, K. *et al.* Magnetic domain walls as reconfigurable spin-wave nanochannels. *Nat. Nanotechnol.* **11**, 432–436. https://doi.org/10.1038/nnano.2015.339 (2016) (**Number: 5 Publisher: Nature Publishing Group**).
7. Wang, Q. *et al.* A magnonic directional coupler for integrated magnonic half-adders. *Nat. Electron.* **3**, 765–774. https://doi.org/10.1038/s41928-020-00485-6 (2020) (**Number: 12 Publisher: Nature Publishing Group**).
8. Krawczyk, M. & Grundler, D. Review and prospects of magnonic crystals and devices with reprogrammable band structure. *J. Phys. Condensed Matter* **26**, 123202. https://doi.org/10.1088/0953-8984/26/12/123202 (2014) (**Publisher: IOP Publishing**).
9. Mathieu, C. *et al.* Lateral quantization of spin waves in micron size magnetic wires. *Phys. Rev. Lett.* **81**, 3968–3971. https://doi.org/10.1103/PhysRevLett.81.3968 (1998) (**Publisher: American Physical Society**).
10. Gallardo, R. A. *et al.* Dipolar interaction induced band gaps and flat modes in surface-modulated magnonic crystals. *Phys. Rev. B* **97**, 144405. https://doi.org/10.1103/PhysRevB.97.144405 (2018) (**Publisher: American Physical Society**).
11. Gallardo, R. A. *et al.* Symmetry and localization properties of defect modes in magnonic superlattices. *Phys. Rev. B* **97**, 174404. https://doi.org/10.1103/PhysRevB.97.174404 (2018) (**Publisher: American Physical Society**).
12. Langer, M. *et al.* Spin-wave modes in transition from a thin film to a full magnonic crystal. *Phys. Rev. B* **99**, 024426. https://doi.org/10.1103/PhysRevB.99.024426 (2019) (**Publisher: American Physical Society**).
13. Lara, A., Robledo Moreno, J., Guslienko, K. Y. & Aliev, F. G. Information processing in patterned magnetic nanostructures with edge spin waves. *Sci. Rep.* **7**, 5597. https://doi.org/10.1038/s41598-017-05737-8 (2017) (**Number: 1 Publisher: Nature Publishing Group**).
14. Zhang, Z. *et al.* Tuning edge-localized spin waves in magnetic microstripes by proximate magnetic structures. *Phys. Rev. B* **100**, 174434. https://doi.org/10.1103/PhysRevB.100.174434 (2019) (**Publisher: American Physical Society**).
15. Caso, D. & Aliev, F. G. Edge spin wave transmission through a vertex domain wall in triangular dots. *SN Appl. Sci.* **4**, 188. https://doi.org/10.1007/s42452-022-05067-z (2022).
16. Hlawacek, G. & Gölzhäuser, A. *Helium Ion Microscopy* (Springer International Publishing, 2016).
17. Hlawacek, G., Veligura, V., van Gastel, R. & Poelsema, B. Helium ion microscopy. *J. Vacuum Sci. Technol. B* **32**, 020801. https://doi.org/10.1116/1.4863676 (2014) (**Publisher: American Vacuum Society**).
18. Lenz, K. *et al.* Trimming of permalloy stripes to enhance the localized edge mode spectrum probed by ferromagnetic resonance. Magnonics 2019, 28.07.-01.08.2019, Carovigno, Italy (2019).
19. Cansever, H. *et al.* Resonance behavior of embedded and freestanding microscale ferromagnets. *Sci. Rep.* **12**, 14809. https://doi.org/10.1038/s41598-022-15959-0 (2022) (**Number: 1 Publisher: Nature Publishing Group**).
20. McMichael, R. D. & Maranville, B. B. Edge saturation fields and dynamic edge modes in ideal and nonideal magnetic film edges. *Phys. Rev. B* **74**, 024424. https://doi.org/10.1103/PhysRevB.74.024424 (2006).
21. Bayer, C. *et al.* Spin-wave excitations in finite rectangular elements of $Ni_{80}Fe_{20}$. *Phys. Rev. B* **72**, 064427. https://doi.org/10.1103/PhysRevB.72.064427 (2005).
22. Körber, L., Quasebarth, G., Otto, A. & Kákay, A. Finite-element dynamic-matrix approach for spin-wave dispersions in magnonic waveguides with arbitrary cross section. *AIP Adv.* **11**, 095006 (2021).
23. Körber, L. *et al.* TetraX: Finite-Element Micromagnetic-Modeling Package, https://doi.org/10.14278/rodare.1418 (2022).
24. Körber, L. *et al.* Symmetry and curvature effects on spin waves in vortex-state hexagonal nanotubes. *Phys. Rev. B* **104**, 184429 (2021).
25. Verba, R., Tiberkevich, V. & Slavin, A. Damping of linear spin-wave modes in magnetic nanostructures: Local, nonlocal, and coordinate-dependent damping. *Phys. Rev. B* **98**, 104408. https://doi.org/10.1103/PhysRevB.98.104408 (2018).
26. Pile, S. *et al.* Nonstationary spin waves in a single rectangular permalloy microstrip under uniform magnetic excitation. *Phys. Rev. B* **105**, 094415. https://doi.org/10.1103/PhysRevB.105.094415 (2022) (**Publisher: American Physical Society**).
27. Sebastian, T., Schultheiss, K., Obry, B., Hillebrands, B. & Schultheiss, H. Micro-focused Brillouin light scattering: imaging spin waves at the nanoscale. *Front. Phys.* **3** (2015).
28. Narkowicz, R., Suter, D. & Niemeyer, I. Scaling of sensitivity and efficiency in planar microresonators for electron spin resonance. *Rev. Sci. Instrum.* **79**, 084702. https://doi.org/10.1063/1.2964926 (2008) (**Publisher: American Institute of Physics**).
29. Banholzer, A. *et al.* Visualization of spin dynamics in single nanosized magnetic elements. *Nanotechnology* **22**, 295713. https://doi.org/10.1088/0957-4484/22/29/295713 (2011) (**Publisher: IOP Publishing**).
30. Cansever, H. *et al.* Investigating spin-transfer torques induced by thermal gradients in magnetic tunnel junctions by using microcavity ferromagnetic resonance. *J. Phys. D Appl. Phys.* **51**, 224009. https://doi.org/10.1088/1361-6463/aac03d (2018) (**Publisher: IOP Publishing**).
31. Lenz, K. *et al.* Magnetization dynamics of an individual single-crystalline Fe-filled carbon nanotube. *Small.* **15**, 1904315. https://doi.org/10.1002/smll.201904315 (2019).
32. Iurchuk, V. *et al.* Data publication : Tailoring crosstalk between localized 1D spin-wave nanochannels using focused ion beams, https://doi.org/10.14278/rodare.2070 (2023).

Acknowledgements

Support by the Nanofabrication Facilities Rossendorf (NanoFaRo) at the IBC is gratefully acknowledged. LK and AK acknowledge the financial support by the Deutsche Forschungsgemeinschaft within the Grants KA 5069/1-1 and KA 5069/3-1. TH and HS acknowledge the financial support by the Deutsche Forschungsgemeinschaft within Program No. SCHU 2922/1-1.

Author contributions

JL conceived the study. JPN and KL performed the FMR experiments. TH conducted the BLS experiments. VI performed micromagnetic simulations with help from LK and AK. RN designed and fabricated the

microresonators. GH performed HIM-assisted milling. VI analyzed the data and wrote the manuscript with help from KL. All co-authors participated in discussions of the results and provided comments to the manuscript.

Funding
Open Access funding enabled and organized by Projekt DEAL.

Competing interests
The authors declare no competing interests.

Additional information
Correspondence and requests for materials should be addressed to V.I.

Reprints and permissions information is available at www.nature.com/reprints.

Publisher's note Springer Nature remains neutral with regard to jurisdictional claims in published maps and institutional affiliations.